Crack closure effects during low cycle fatigue propagation in line pipe steel: An analysis with digital image correlation

S. Rabbolini [a,*], S. Beretta [a], S. Foletti [a], M.E. Cristea [b]

[a] *Department of Mechanical Engineering, Politecnico di Milano, Via La Masa, 1, Milan 20156, Italy*
[b] *TenarisDalmine R&D – Structural Integrity Department, Dalmine SpA, Piazza Caduti 6 Luglio 1944, 1, Dalmine, BG 24044, Italy*

Received 13 January 2015
Received in revised form 1 July 2015
Accepted 24 July 2015
Available online 1 September 2015

1. Introduction

Pipelines are employed in challenging harsh environments, where they have to sustain severe loading conditions. Especially when working in arctic-like environments, linepipe materials can be subjected to plastic straining cycles due to thermal cycling between service and shutdown and to occasional large plastic deformations induced by ice scouring in shallow water [1–3].

Fatigue properties (fatigue strength and life) can be conservatively predicted, assuming the presence of small shallow cracks with a depth corresponding to the detection limit of Non-Destructive Techniques (NDT) [4]. Therefore, an initial assessment of pipelines fatigue properties can be made considering a crack propagation problem in the Low Cycle Fatigue (LCF) regime, in which a crack starts propagating from the first load cycle [5]. Due to the presence of high plastic strains, traditional approaches based on Linear Elastic Fracture Mechanics (LEFM) cannot be applied in LCF [6]. On the other hand, crack growth rates in the LCF regime can be described as a function of the cyclic J-Integral, ΔJ. The idea to extend Rice's path independent J-Integral [7] to fatigue was originally proposed by Dowling [8], who modified Paris relationship [9], by replacing with ΔJ the stress intensity factor range, ΔK. ΔJ formulation was employed to analyze crack growth in the early propagation phase in [10], whereas in [11] a model based on the cyclic J-Integral was adopted to provide an assessment of fatigue life of specimens tested under LCF loading conditions. Such an approach was also adopted by Skallerud and Zhang for describing the growth of flaws in off-shore components under extremely high strain levels (prospective LCF life of 80–100 cycles under $\Delta\epsilon > 2\%$ [12]).

* Corresponding author.
E-mail address: silvio.rabbolini@polimi.it (S. Rabbolini).

Nomenclature

A_0	extension of the plastic zone surrounding the crack-tip
A_n	extension of the infinitesimal part of the plastic zone surrounding the crack-tip
a	crack length
a_0	initial crack length
a_f	crack length to failure
$2\ c$	surface crack extension
C, m	Paris law constants
$h(n_i)$	function for plastic J-Integral range description
k_i	cyclic strain/stress curve constant
n_i	cyclic strain/stress curve exponent
E	Young's modulus
R	strain ratio ($\epsilon_{min}/\epsilon_{max}$)
R_m	ultimate tensile strength
$R_{p,02\%}$	yield stress
$R'_{p,02\%}$	cyclic yield stress
Y	geometric factor
ΔJ	cyclic J-Integral
ΔJ_{el}	elastic part of the cyclic J-Integral
ΔJ_{pl}	plastic part of the cyclic J-Integral
ΔJ_{eff}	effective J-Integral range
ΔK	stress intensity factor range
ΔK_{eff}	effective stress intensity factor range
ΔW_e	elastic strain energy density
ΔW_p	plastic strain energy density
$\Delta\sigma$	stress range
$\Delta\sigma_{eff}$	effective stress range
$\Delta\epsilon$	strain range
$\Delta\epsilon_{eff}$	effective strain range
$\Delta\epsilon_p$	plastic strain range
$\Delta\epsilon_{p,eff}$	effective plastic strain range
α	constraint factor
$\epsilon_{a,p}$	plastic strain amplitude
ϵ_{el}	elastic part of the total strain
ϵ_{max}	maximum strain during the fatigue cycle
ϵ_{op}	strain measured at crack opening
ϵ_{pl}	plastic part of the total strain
σ_0	flow stress
σ_n	stress in the direction normal to crack plane
σ_{cl}	crack closing stress
σ_{max}	maximum stress during the fatigue cycle
σ_{open}	crack opening stress
σ_{ref}	reference stress for data normalization

It has been shown that, at lower strain amplitudes, crack closure is an important factor, even during LCF crack growth. Seeger and Vormwald [13–15] measured crack opening levels during LCF experiments by placing a strain gage over the crack and measuring the changes in local strains. Starting from these observations, they proposed a different formulation of ΔJ, which implemented the effects of crack closure. The cyclic J-Integral equation was modified by replacing stress and plastic strain ranges with the effective ones, calculated by considering only the portion of the fatigue cycle in which the crack stays open. A similar approach was also proposed by McClung and Sehitoglu in [16,17] and by Pippan and Grosinger in [18]. In[19], ΔJ_{eff} formulation was rewritten and successfully applied to describe crack propagation under LCF at high temperature.

In these models, crack closure was modeled by means of the equations proposed by Newman [20]. The adoption of the model proposed by Newman, however, presents some limitations, since it was developed for cracks propagating under LEFM conditions and considering fully reversed loads.

In this work, crack closure mechanisms are investigated by adopting a recent technique based on computer vision, Digital Image Correlation (DIC). DIC was initially developed in the early 1980s at the University of South Carolina [21–24], with the idea to measure full-field in-plane displacements and displacement gradients of a strained body, but was also successfully applied to fracture mechanics. In [25,26], DIC was employed to characterize opening and closing levels by measuring the

relative displacements of crack flanks during a fatigue cycle. Recently, DIC was employed to measure the displacements in the area surrounding the tips. These displacements were employed to extract crack propagation driving forces [27–29], by fitting the experimental displacements with the analytical singular field. This approach, however, is not suitable for LCF propagation, since it is based on LEFM equations. Therefore, in this paper, a different technique capable of measuring crack closure effects in zones affected by large plastic strains is presented, with the aim to provide a deep analysis of crack closure mechanisms in presence of high plastic strains.

From this background, the effect of severe strain cycles onto line pipe steel was analyzed as propagation of prospective flaws in the very Low Cycle Fatigue (LCF) regime. The propagation of short cracks was measured together with DIC measurements of the closure levels. This allowed us to obtain a crack growth model based on ΔJ_{eff} concepts.

1.1. Plan of the activity

The aim of the present research was to develop a crack propagation model for materials subjected to severe strain cycles adopting the ΔJ_{eff} concepts. The following experiments were carried out:

- Short crack propagation on small scale specimens. In this phase, specimens (with a net section of 12 mm × 7 mm) with artificial semi-circular artificial defects with a depth of 400 μm were cyclically loaded under LCF. This first series of experiments was performed in order to analyze material cyclic behavior and the crack growth rate by means of closure measurements with DIC;
- Short crack propagation on large scale specimens. Crack closure levels were measured during fatigue tests performed on specimens with a net section of 43 mm × 10 mm and the presence of shallow micronotches (depth to width equal to 1:10), in order to have constraint levels similar to those of shallow surface cracks on pipelines.

The first phase allowed us to set-up a crack growth model that was successfully validated by the crack growth experiments on large scale specimens.

2. Crack propagation models under LCF

As it will be seen in the following sections, severe cycling conditions correspond to fatigue cycles up to 1% plastic strains. Therefore, it is important to analyze the prospective propagation of potential defects in presence of significant plastic strain cycles.

Fatigue crack growth under LCF conditions can be described following two different approaches. The first one, originally proposed by Tomkins [30], correlates crack growth rates to the applied plastic strain amplitude, $\epsilon_{a,p}$. Such an approach is the fundamentals of the short crack propagation model included in the british R6 procedure [31]. It has been proved [32] that such an approach provides good results only when large strains are considered, whereas it looses accuracy when $\epsilon_{a,p}$ tends to zero, leading to a non-conservative prediction.

The second approach is based on Elastic–Plastic Fracture Mechanics (EPFM). In these models, crack propagation is described as a function of the cyclic J-Integral. Several formulation of ΔJ have been proposed [10,11]. The general formulation of ΔJ can be expressed as a function of the elastic and the plastic strain energy density [19]:

$$\Delta J = f(\Delta W_e) + g(\Delta W_p) = \pi Y^2 a \left[(1-\nu^2)\frac{\Delta\sigma^2}{E} + h(n_i)\Delta\sigma\Delta\epsilon_p \right] \tag{1}$$

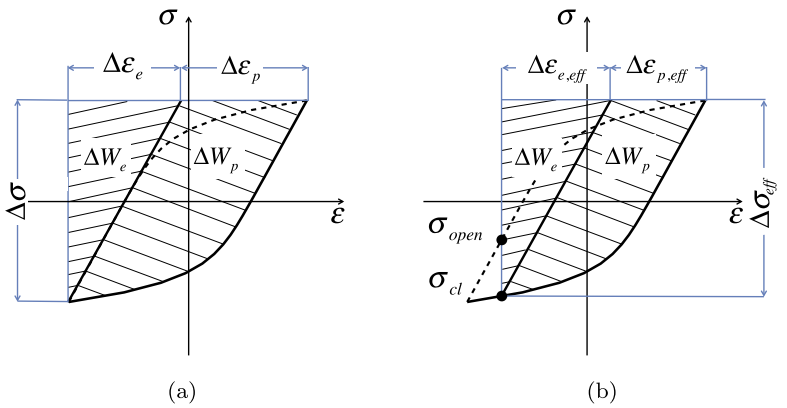

Fig. 1. Schematic illustration of the notable points necessary to determine ΔJ (a) and ΔJ_{eff} (b).

where ΔW_e and ΔW_p are, respectively, the elastic and plastic strain energy densities, as reported in Fig. 1a, Y is a factor that accounts for crack geometry, a is the crack length, ν is the Poisson's ratio, $\Delta\sigma$ is the applied stress range, E is Young's modulus, $\Delta\epsilon_p$ is the plastic strain range, n_i is the cyclic stress/strain curve exponent and $h(n_i)$ is a function that takes into account crack geometry and material elastic–plastic behavior.

The original formulations based on ΔJ have been later modified, in order to take into account crack-closure effects, since it has been shown that this phenomenon is an important factor even in LCF [13,16]. The effects of crack closure can be implemented in ΔJ equation by reducing stress and strain ranges, considering only the part of the fatigue cycle in which the crack stays open. The general formulation of the effective cyclic J-Integral, ΔJ_{eff}, is obtained by replacing in Eq. (1) $\Delta\sigma$ and $\Delta\epsilon_p$ with $\Delta\sigma_{eff}$and $\Delta\epsilon_{p,eff}$, the effective stress and plastic strain ranges:

$$\Delta J_{eff} = \pi Y^2 a \left[(1-\nu^2)\frac{\Delta\sigma_{eff}^2}{E} + h(n_i)\Delta\sigma_{eff}\Delta\epsilon_{p,eff} \right] \tag{2}$$

In this work, the model proposed by Vormwald and Seeger [13–15] is considered. According to this model, crack opening levels are calculated by applying the equations proposed by Newman [20] for long cracks, in which σ_{open}, for a given stress ratio, depends on the constraint factor α, related to crack geometry and remote loading conditions, and to the ratio between σ_{max}, the peak stress, and σ_0, the flow stress. It has been shown [13,16] that conservative assessments of crack opening levels can be obtained by setting α equal to 1, together with a value of σ_0 calculated as expressed in Eq. (3), where $R'_{p,02\%}$ is the cyclic yield stress and R_m is the ultimate tensile strength.

$$\sigma_0 = \frac{1}{2}\left(R'_{p,02\%} + R_m\right) \tag{3}$$

In their model, Vormwald and Seeger [13–15], assumed that crack opening and closing, during LCF, occur at the same strain level: therefore, σ_{cl}, the crack closing stress, is calculated as the stress reached, during unloading, when the strain at crack-opening, ϵ_{op}, is reached. Consequently, effective stress and plastic strain ranges are calculated as:

$$\begin{aligned} \Delta\sigma_{eff} &= \sigma_{max} - \sigma_{cl} \\ \Delta\epsilon_{p,eff} &= \epsilon_{max} - \epsilon_{op} - \frac{\Delta\sigma_{eff}}{E} \end{aligned} \tag{4}$$

A summary of the significant points of Vomwald and Seeger's model is reported in Fig. 1b, in which the two hatched areas represent the elastic and plastic strain energy densities considered in ΔJ calculation, following Dowling's original proposal [33].

The approach based on ΔJ_{eff} is consistent with Tomkins' model, since at high strains σ_{open} tends to 0. Thus, $\Delta J_{eff} = \Delta J$ and ΔJ is controlled by $\Delta\epsilon_p$.

3. Fatigue crack growth in small scale specimens

3.1. Material response under severe cycling

The activity carried out on heavy wall linepipes [1–3] identified a critical cycling sequence. Cycling has been defined as the superposition of one strain ramp in plastic range, up to 1%, superposed to a sub-cycling at 0.5% of total strain, for a limited number of cycles (≈200). These straining cycles aim at reproducing situations that can occur during pipeline life in artic-like environments.

Different LCF tests were carried out on a sour service grade API 5L X65Q steel for heavy wall linepipes (detailed informations on the metallurgical design and typical properties of this material are reported in [34,35]). In order to set-up a crack propagation model for prospective flaws in linepipes subjected to those severe straining cycles, LCF were carried out in two conditions:

- strain cycles from 1% to 0.5%;
- strain cycles at $R = -1$ with $\epsilon_a = 0.35\%$.

The latter test condition was chosen as a reference condition, since a good performance of the ΔJ_{eff} model is usually obtained under fully reversed strain cycles [19].

In Fig. 2, the material cyclic behavior, recorded during the experiments performed under the two different strain conditions, is reported. Due to confidentiality issues, experimental results are presented in a normalized form (i.e. all the stresses were normalized by a reference stress, σ_{ref}). Material exhibits a transient behavior. In particular, mean stress relaxation is observed during the tests performed at $R = 0.5$, as depicted in Fig. 2a. After 500 cycles, the applied mean stress tends to zero.

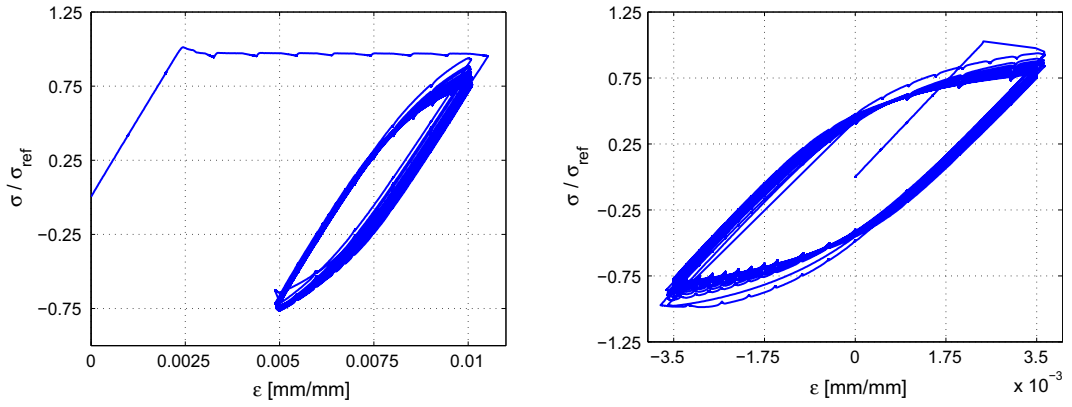

Fig. 2. Hysteresis loop evolution during LCF testing. (a) Test performed at $R = 0.5$ and ϵ_a = 0.0025 mm/mm; (b) Test performed at $R = -1$ and ϵ_a = 0.0035 mm/mm.

3.2. Specimen preparation

An experimental campaign was carried out to observe crack propagation in specimens containing artificial notches. 0.4 mm deep semi-circular defects, obtained by Electrical Discharge Machining (EDM), were employed during the experi-ments. The geometry of the specimens used for testing is reported in Fig. 3a, in which artificial defect shape and orientation are also shown. Tests were performed on a 100 kN servo-hydraulic load frame: a longitudinal extensometer, with a 10 mm gage length, was employed to control the applied strain amplitudes. The experimental setup is shown in Fig. 3b.

Before testing, specimens were precracked in compression, in order to obtain a sharp fatigue crack. Precracking was deemed necessary, in order to remove crack nucleation time from the experiments. The compression pre-cracking constant amplitude (CPCA) technique, originally proposed by Newman [36], was employed in this phase. According to this technique, after compression pre-cracking the crack reaches the same size of the plastic zone generated around the notch during the first compressive load cycle. A numerical analysis of one quarter of the specimen was performed to calculate the load that causes a plastic region of 100 μm, the desired size of the precrack. The simulation was performed with the FEA solver Abaqus, by Dassault Systemes, by adopting a traditional Von Mises plasticity model. It was found that a remote compressive stress of 400 MPa generates a region of 120 μm ahead of the notch with positive residual stresses. Therefore, specimens were pre-cracked in compression, with an applied mean stress equal to −200 MPa and a stress amplitude equal to 200 MPa. It was observed that all the specimens, after precracking, exhibited an average 100 μm long defect extending from both the sides of the EDM notch, confirming the numerical observations.

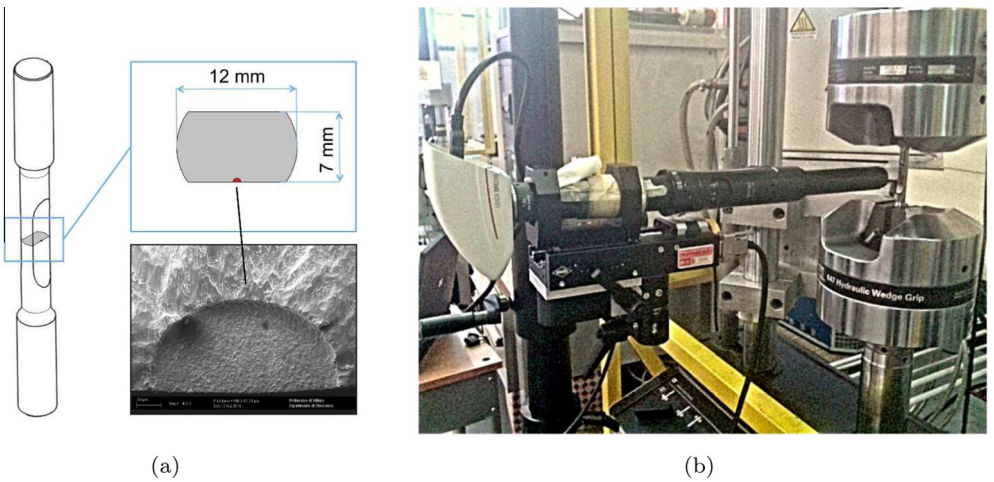

Fig. 3. LCF testing under severe loading conditions. (a) Specimen geometry of the small scale specimen (notch depth equal to 0.4 mm); (b) Experimental setup with the digital camera employed to observe crack propagation during the experiment.

3.3. Fatigue tests

Four samples were cyclically loaded: constant strain amplitude tests were performed under the loading conditions described in the previous section. One specimen was tested at $R = -1$, whereas the other three were loaded at $R = 0.5$, the most demanding in-service condition. All the tests were performed with a frequency of 0.5 *Hz* and were interrupted when a surface crack length equal to 2 mm was reached.

A fifth specimen was tested at $R = 0.5$: this test was interrupted after 200 cycles, in order to analyze the fracture surface in the early propagation stage. The analysis of the fracture of this specimen, conducted with a Scanning Electron Microscope (SEM), is reported in Fig. 4a, where it can be seen that the crack initially propagates in the direction of the plastic zone generated by the first strain step.

Crack length was measured during tests interruptions by adopting two different techniques: defect size was initially measured with the plastic replica technique discussed in [37]: an example of the fracture surface is presented in Fig. 4b. The so-obtained crack lengths were then compared to those measured from the pictures acquired by an HD digital camera, whose resolution was 1600 $\times$ 1200 pixels. After the end of the first test, crack length was measured only from the digital images, since this technique provided satisfactory results and it allowed to reduce the time required for testing. A magnifi-cation of 15$\times$, obtained using an adjustable lens with a 6.5$\times$ magnification range and a 10$\times$ adapter, was employed during the experimental campaign. This setup allowed a resolution of 2 μm/pix.

After the end of the tests, all the specimens were broken in liquid nitrogen in order to observe the final shape of the defect. Since all the specimens exhibited a semi-circular fatigue crack, as shown in Fig. 4c, it was assumed that the aspect ratio remained constant during propagation (i.e. $a/c = 1 = const.$). Therefore, the defect size, a, was calculated as one half of the surface defect size, $2c$, and experimental crack growth rates, da/dN, were then derived by applying the *secant method*.

3.4. Analysis of experimental results

Experimental results were analyzed considering the model based on ΔJ_{eff} proposed in [13–15] and described in Section 2. The effects of crack closure were considered by applying the model proposed by Newman. A geometric factor, Y, equal to $2/\pi$, and a correction function, $h(n_i)$ equal to $3/(4\sqrt{n_i})$ were considered in this analysis, following Vormwald's proposal.

Experimental results were compared to the crack propagation curve obtained from a C(T) specimen tested at a high stress ratio ($R = 0.7$), as reported in Fig. 5. It was found that experimental data-points do not lie on the crack propagation curve: in particular, experimental data points showed an unexpected increase in crack growth rates. A wrong estimation of crack

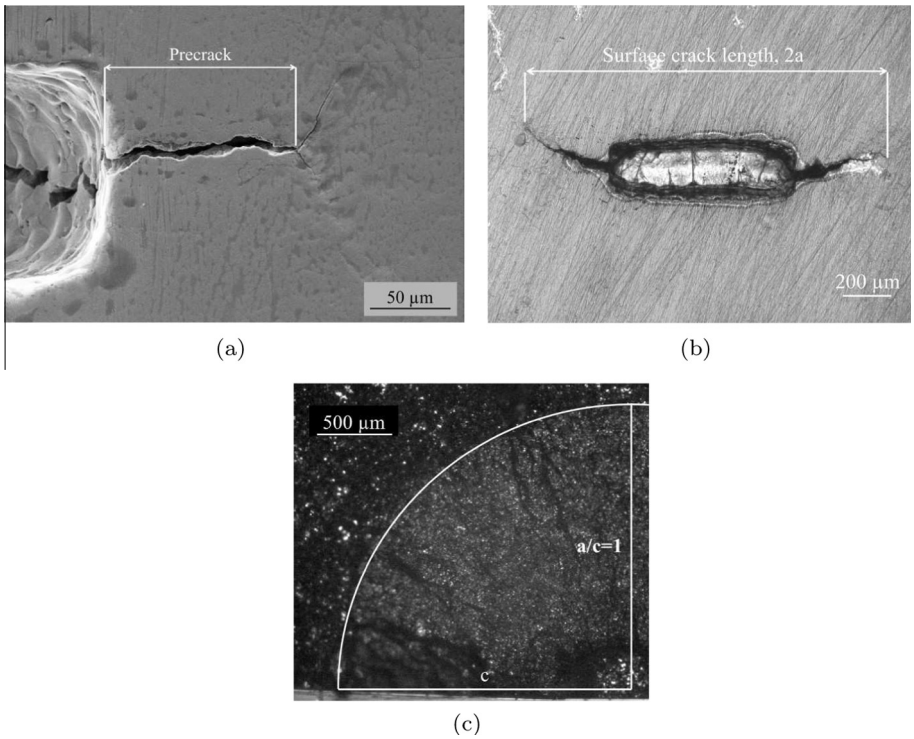

Fig. 4. Fracture surfaces during fatigue crack growth. (a) Fracture surface in the early propagation stage; (b) Surface crack propagation on a sample surface, observed on a plastic replica; (c) Fatigue crack surface after the end of the experiment.

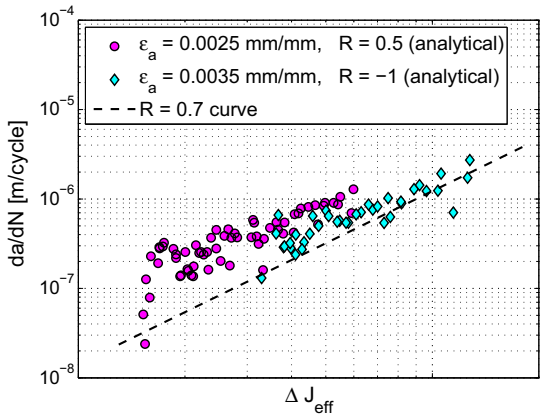

Fig. 5. Fatigue crack growth analysis based on ΔJ_{eff} [13]. Crack opening and closing levels calculated according to Newman [20].

opening and closing levels can be responsible for this increment, since it changes the value of the effective stress and strain ranges, implying a reduction of the calculated ΔJ_{eff}: a new experimental campaign was performed in order to evaluate crack closure levels. The results of this analysis are reported in the following section.

4. Crack closure measurements in LCF with digital image correlation

4.1. Experiments and digital image correlation procedure

An experimental campaign was performed in order to measure crack opening and closing levels during short crack propagation. Crack closure was characterized with Digital Image Correlation (DIC). Four experiments were conducted on the specimen geometry presented in Fig. 3a: the first two tests were performed at $R = -1$, whereas the remaining two were cyclically loaded at $R = 0.5$, considering the strain amplitudes discussed in Section 3. The final surface crack length, necessary to consider a test as concluded, was increased to 4 mm, in order to acquire more datapoints. Before testing, specimens were prepared by manually polishing the surface to a mirror finish with abrasive paper, up to a grit of P2500. A speckle pattern, necessary for digital image correlation, was painted onto each specimen with an airbrush, following the procedure discussed in [27,28,38]. During test interruptions, necessary to measure crack advancement, a fatigue load cycle was manually performed in order to acquire several pictures of the crack. Vertical and horizontal displacements were then calculated by correlating the images taken during the fatigue cycle with the reference image, which was the first picture of each measurement cycle, acquired at the minimum applied strain. These displacement fields were the starting point of the crack closure measurements presented in the following section.

4.2. Virtual strain gauges

A new technique was implemented in order to evaluate crack closure. In one of their works [13], Vormwald and Seeger proposed an experimental technique to measure crack opening and closing levels during constant strain amplitude tests. This technique consists in placing a strain gage as close as possible to a fatigue crack: the so-measured local stress/strain cycle is compared with the global one, which is the fatigue cycle measured by the external extensometer, which controls test execution. Crack opening and closing levels can be estimated as the points in which local and global hysteresis loops start to differ. The difference between global and local behavior is related to the change of specimen compliance: when the crack stays closed, the zone surrounding the fracture behaves in the same way of those parts far from the defect, whereas it looses stiffness when the crack starts opening. In particular, when the crack stays open, the strains locally measured are smaller than those remotely recorded, since the gage stays in the strain shadow of the crack.

In this work, crack closure effects were experimentally investigated through a similar approach, but using an innovative technique based on DIC. Initially, a 300 μm- wide series of virtual strain gages was positioned under the EDM notch, as proposed in Fig. 6a, in which the vertical strains measured around a 0.8 mm long crack subjected to a remote strain of 0.0035 mm/mm are reported. The gauges were set to read axial strains, following Vormwald's original proposal. The measurements provided by the virtual gage are compared to the remote strains measured by the extensometer in Fig. 6b: this approach does not provide any result, since that part of the specimen does not carry any load. Trying to obtain a correct estimate, the strain gauge was moved in the cyclic plastic zone, very near to the crack tip, as depicted in Fig. 6c: the strains evaluated in this zone are depicted in Fig. 6d, where it can be seen that even in this case it is not possible to assess opening and closing levels, due to the high strains present near the tip.

In order to get an accurate measurement, the virtual strain gauge was moved between the cyclic plastic zone and the notch (Fig. 7a): the strain values measured in this zone can be used to calculate crack opening and closing levels, as it

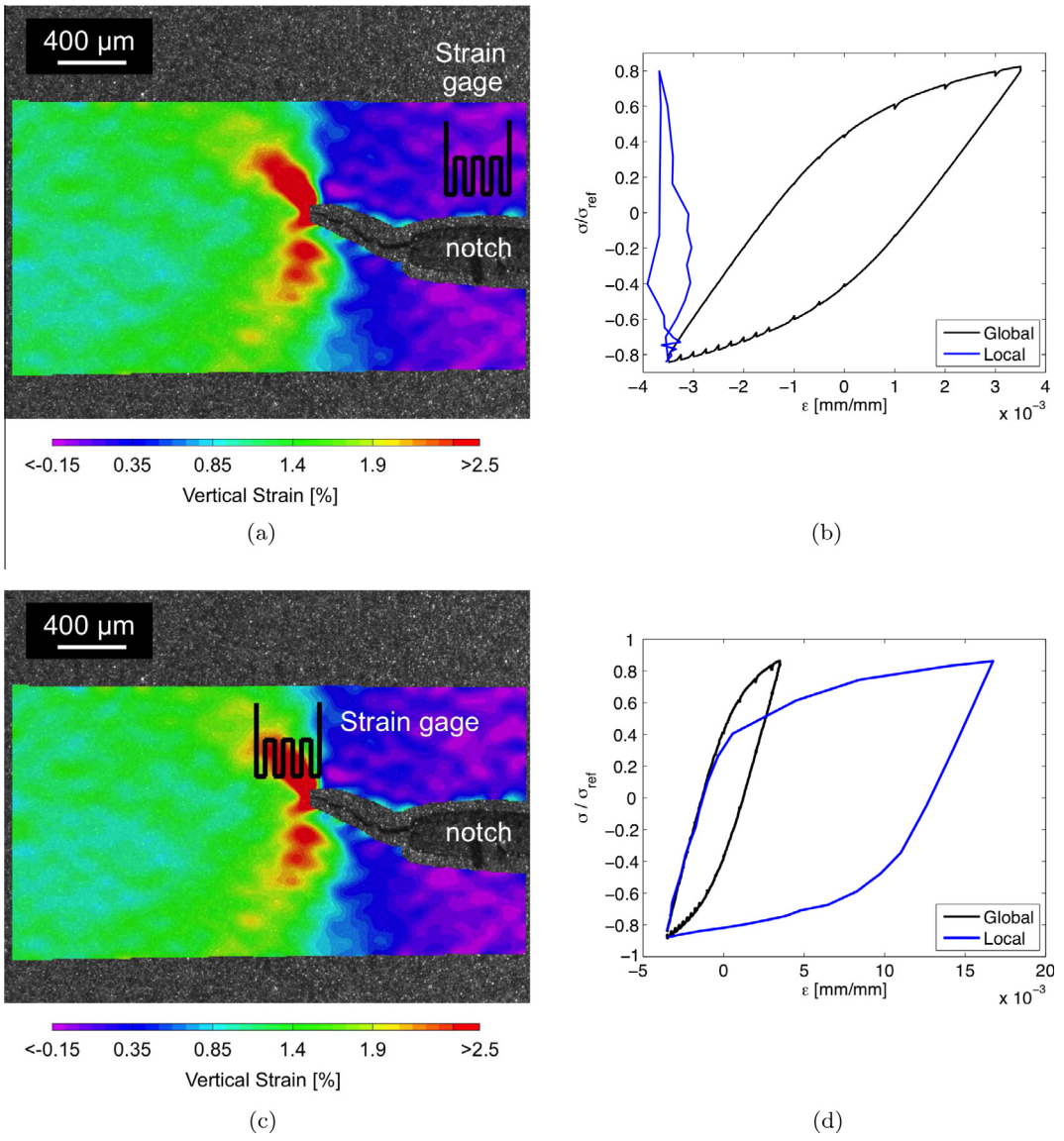

Fig. 6. Crack closure measurements in LCF with DIC. (a) Virtual strain gauge position, Vormwald's proposal [13]; (b) Local stress/strain loop measured under the EDM notch; (c) Virtual strain gauge position near crack-tip. (d) Local stress/strain loop measured in the cyclic plastic zone.

can be seen in Fig. 7b. Moreover, the method showed to be consistent: a 50 μm change in the horizontal position of the strain gauge did not affect the recorded closure levels, confirming the extracted closure values.

This technique, however, present a limitation, related to the applied loading conditions: the presence of high strain implies a great vertical displacement of the measurement surface. This means that the magnification employed for image acquisition is limited by the vertical travel of the defect during the fatigue cycle and that only a small portion of the area surrounding the tip can be monitored. During the experiments, it was found that for the current setup the maximum allowable magnification, satisfactory for DIC measurements, is 30, which corresponds to a resolution of 1 μm/pix.

At this point, the technique was applied to the experiments, positioning the virtual strain gauges at 150 μm from crack-tip, since it was found that this position provides best results: an example of the crack closure measurements, obtained during small scale testing, is provided in Fig. 8a and b. Crack opening and closing levels can be easily recognized and occur at the same strain level. These observations confirm the measurements presented by Vormwald [13] and the validity of his concept.

4.3. Results

Experimental results were compared to those obtained considering Newman's analytical model, in terms of $\Delta\sigma_{eff}/\Delta\sigma$. The effective stress range was calculated according to Eq. (4). As it can be seen in Fig. 9a, the model, when $R = -1$ tests are considered, correctly estimates the value of the effective stress range, providing a small error (≈5%). On the other part,

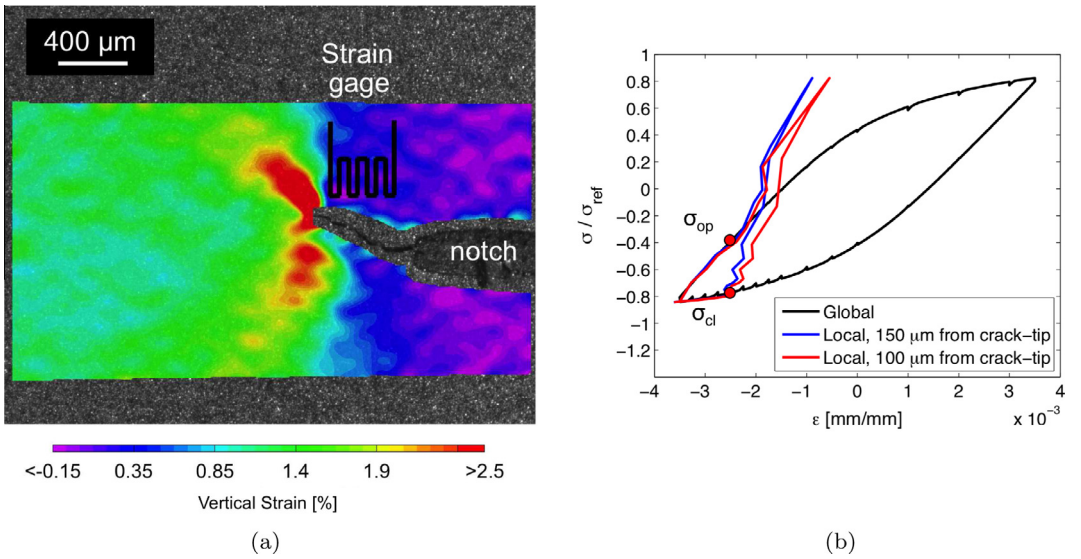

Fig. 7. Crack closure measurements in LCF with DIC. (a) Virtual strain gauge position adopted for crack closure estimates; (b) Comparison between local and global hysteresis loops and opening and closing levels identification.

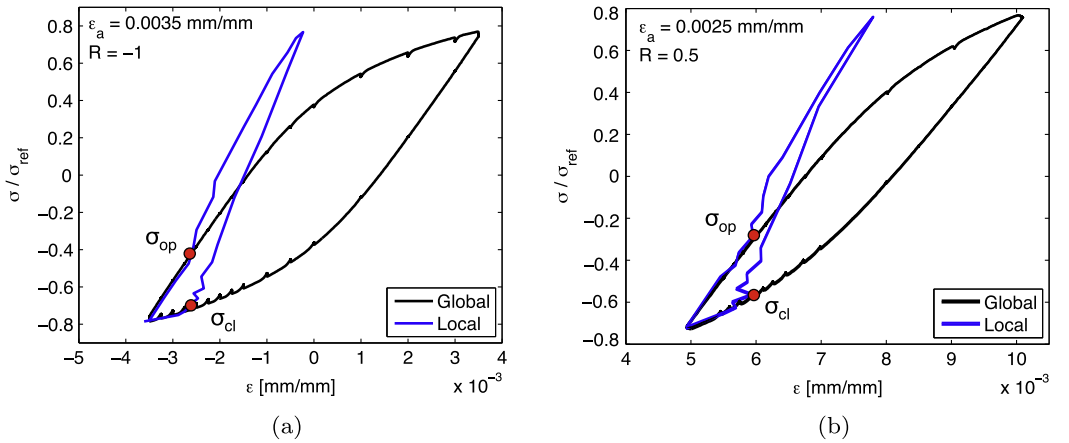

Fig. 8. Crack closure measurements in LCF with DIC on small scale specimens. (a) Comparison between local and global hysteresis loops and opening and closing levels identification for tests conducted at $R = -1$; (b) Comparison between local and global hysteresis loops and opening and closing levels identification for tests conducted at $R = 0.5$.

greater errors are present when tests with a mean strain are considered (Fig. 9b). In particular, for those tests performed at $R = 0.5$, the model underestimates the value of $\Delta\sigma_{eff}$: this implies that a procedure based on Newman's formulation underestimate the applied effective J-Integral range. In order to verify if the model can be improved, a different formulation of the flow stress was implemented [39]: the value of σ_0, calculated according to Eq. (3), was replaced by the cyclic yield stress. This new formulation, represented in Fig. 9 by a dashed line, offers a small improvement, since it increases the value of $\Delta\sigma_{eff}$ in both the considered conditions, but it still provides wrong estimates when tests with an applied mean strain are considered.

In Fig. 10, experimentally observed crack growth rates are plotted against the effective J-Integral ranges, calculated considering the effective stress and strain amplitudes measured with DIC: all the experimental points collapse on a single curve, which has the same trend of the da/dN–ΔK_{eff} curve obtained testing a C(T) specimen at high load ratio ($R = 0.7$).

5. Fatigue crack growth in large scale specimens

5.1. Experiments

The experimental analysis of fatigue crack growth on small scale specimens underlined the capability of ΔJ_{eff} based models to accurately describe crack propagation under severe loading conditions. At this point, four larger specimens were tested, in order to check the propagation model when artificial defects with an aspect ratio similar to the one observed in the pipelines are present. A schematic of the specimen used for testing, together with the shape and the orientation of the

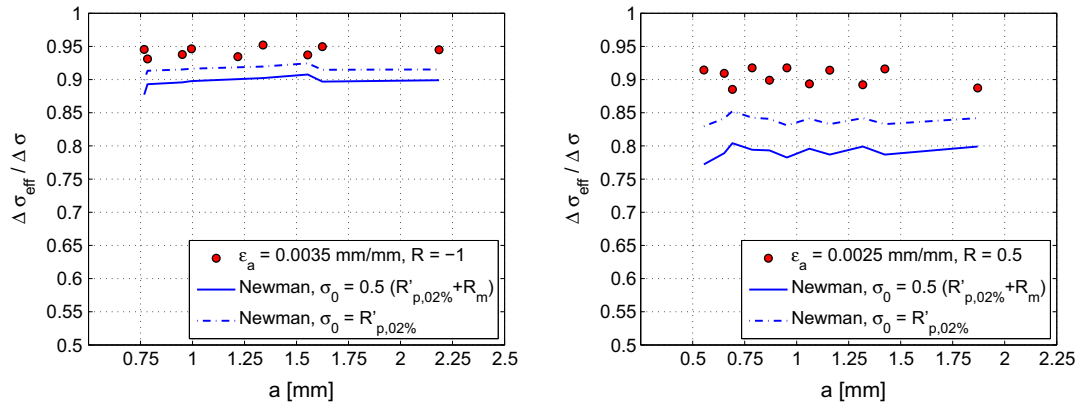

Fig. 9. Comparison between experimental and analytical effective stress amplitudes, small scale specimens. (a) $R = -1, \epsilon_a = 0.0035$ mm/mm; (b) $R = 0.5, \epsilon_a = 0.0025$ mm/mm.

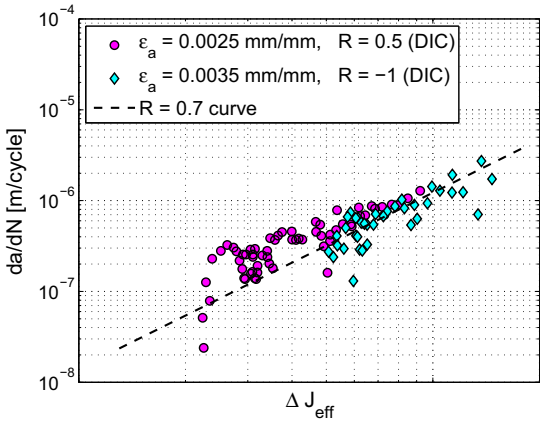

Fig. 10. Fatigue crack growth analysis based on ΔJ_{eff} [13]. Crack opening and closing levels calculated from DIC measurements.

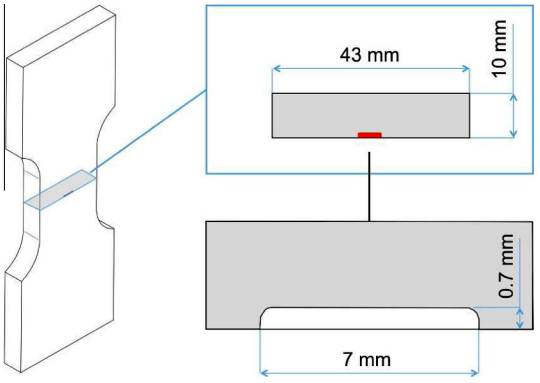

Fig. 11. Specimen geometry of the large scale specimen.

artificial defect, is presented in Fig. 11. The defects adopted in this phase were 7 mm wide and 0.7 mm deep. In the following, this geometry will be referred as *large scale*.

Before testing, specimen were prepared following the procedure discussed in the previous section: initially, specimens were mechanically polished, painted and then precracked in compression. At this point, specimens were tested in a 250 kN servo hydraulic load frame. A longitudinal extensometer, with a 20 mm long gage, was employed to control the applied

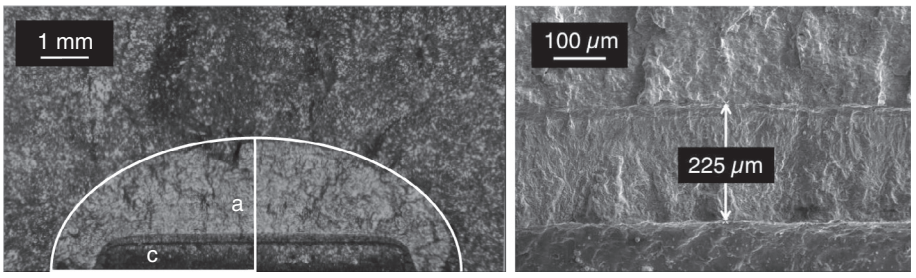

(a) (b)

Fig. 12. Fracture surface of a large scale specimen tested for 250 cycles at $R = -1$ and $\epsilon_a = 0.0035$ mm/mm. (a) Semi-elliptical fatigue crack after the end of the test; (b) SEM detail of the precrack.

strain amplitude. Specimens were cyclically loaded adopting the same levels discussed in Section 3. Two tests for each loading condition were performed.

After the end of the tests, specimens were broken in liquid nitrogen, to observe the final shape of the fatigue crack and to highlight the difference in propagation between the superficial and the deepest points of the crack. In Fig. 12, an example of a fracture surface observed after a fatigue test conducted at $R = -1$ is reported. The crack shape (Fig. 12a) is completely different from the initial notch geometry. In particular, a semi-elliptical defect can be observed: this is due to the fact that, on the surface, crack propagation occurs at slower rates, since crack opening and closing levels are higher because of the plane stress condition acting in these regions. Compression precracking generates a 225 μm fatigue crack around the notch, as reported in Fig. 12b. It is worth remarking that the aspect ratio of the defect is changing during the test, because of the different crack growth rates experienced at the different points along crack flanks. A final average aspect ratio, a/c, of 0.75 was calculated for the specimens tested in this phase. The different crack growth rates along the crack front, together with the small number of specimens tested, made it impossible to obtain a relationship between a and c. This neglected the possibility to obtain a graph like the one proposed in Fig. 10.

5.2. Results

Crack opening and closing levels were measured according to the technique presented in Section 4. 300 μm wide strain gauges were positioned following what proposed in Fig. 7, since small scale testing showed that this position can provide accurate closure measurements. In Fig. 13, two selected fatigue load cycles, employed for crack closure analysis, are reported. A measurement cycle obtained from $R = -1$ testing is reported in Fig. 13a: the experimental technique is cabaple of measuring the crack opening level, but the method looses accuracy when the descending part of the hysteresis loop is considered. The same observations can be made considering the measurement cycle obtained from $R = 0.5$ testing (Fig. 13b). This can be related to the fact that DIC allows to measure crack opening and closing levels only on the surface of the specimens. It can be assumed that the plane stress condition occurs for these external points, whereas the remaining

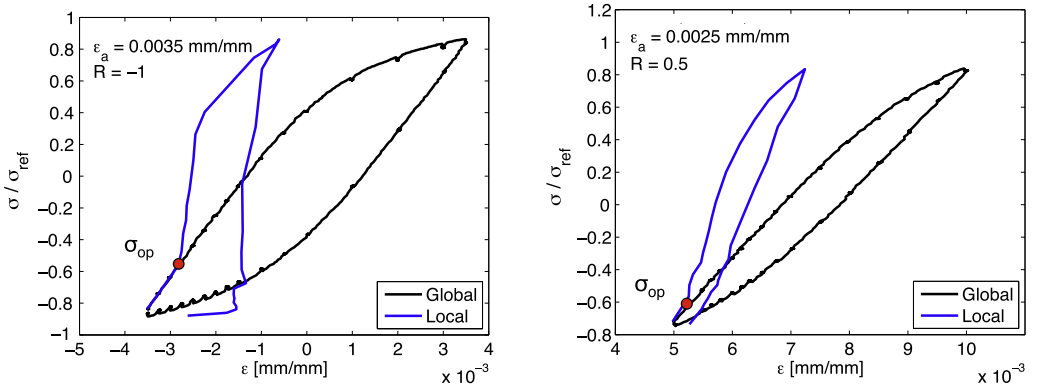

(a) (b)

Fig. 13. Crack closure measurements in LCF with DIC on large scale specimens. (a) Comparison between local and global hysteresis loops and opening and closing levels identification for tests conducted at $R = -1$; (b) Comparison between local and global hysteresis loops and opening and closing levels identification for tests conducted at $R = 0.5$.

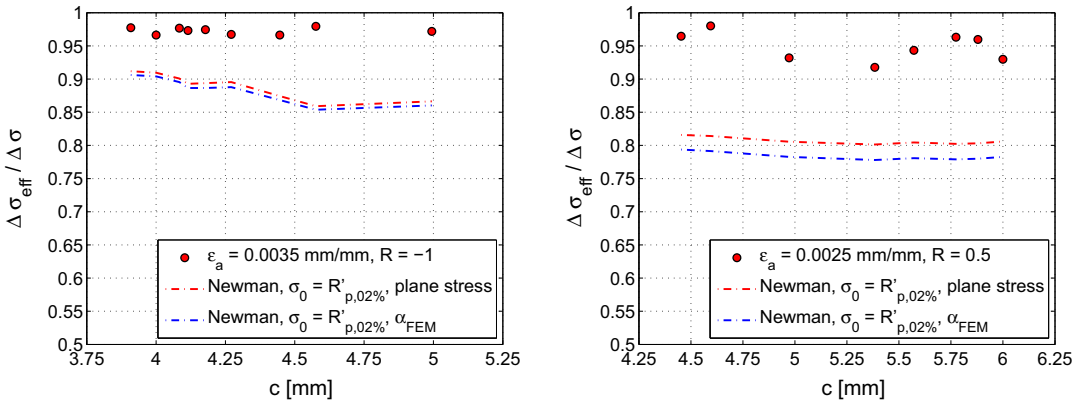

Fig. 14. Comparison between experimental and analytical effective stress amplitudes, large scale specimens. (a) $R = -1, \epsilon_a = 0.0035$ mm/mm; (b) $R = 0.5, \epsilon_a = 0.0025$ mm/mm.

part of the crack front is experiencing a stress condition similar to plane strain. This means that crack opening and closing levels are different along the crack front. In particular, the plane stress condition implies that surface points tend to open and close at stresses higher than those registered for the central points of the crack. Consequently, during unloading, the external points are the first to experience crack closing: in these conditions, measurements are disturbed by the stress fields generated by the contact occurring in those zones where plane strain condition is present. This feature is not present in the small scale specimens, since the crack front is smaller and it can be assumed that all the point lying on the crack front experience the same opening and closing levels.

In order to evaluate the values of $\Delta\sigma_{eff}$, it was assumed that crack closing occurred at the same strain level registered at opening, following what was experimentally observed on the small scale specimens and Vormwald's hypotheses. Experimental results, expressed in terms of $\Delta\sigma_{eff}/\Delta\sigma$, are reported in Fig. 14, where, for both the loading conditions investigated, it can be observed that the measured values of $\Delta\sigma_{eff}$ are higher than those registered during small scale testing. This is related to the fact that the constraint condition recorded in the large scale specimen geometry is more severe than the one of the small scale specimen. In particular, it can be noted that the ratio between $\Delta\sigma_{eff}$ and $\Delta\sigma$ is very close to 1, meaning that the crack stays open for almost the entire fatigue cycle.

5.3. Analysis of constraint

The observation of the crack shape after the experiments underlined the fact that the constraint factor, α, is changing along the crack front. In order to evaluate the loading condition present at the crack deepest point and to evaluate opening and closing levels according to Newman's analytical model, a FEM model was developed to calculate α.

According to Newman [40], the constraint factor can be calculated as reported in Eq. (5), in which σ_n is the value of the stress in a point of the plastic zone surrounding the tip, dA is an infinitesimal part of the total plastic zone, A_0, and σ_0 is the flow stress, calculated following Vormwald's proposal (Eq. (3)). In order to evaluate α from the FE analysis, the plastic zone was divided into small sectors, whose area was A_i, in which the stress, $\sigma_{n,i}$, was supposed to be constant and equal to the nodal value. It was found that, for the given geometry, $\alpha = 1.434$.

$$\alpha = \frac{\int_{A_0} \sigma_n dA}{\sigma_0 \cdot A_0} \approx \frac{\sum_i \sigma_{n,i} \cdot A_i}{A_0 \sigma_0} = 1.434 \tag{5}$$

At this point it was possible to calculate the analytical values of the effective stress ranges. In Fig. 14, analytical values are compared to those experimentally measured. In this case, only the formulation of the flow stress proposed by Savaidis was considered. In order to observe the influence of the constraint factor on the crack opening levels, two different values of α were considered. In particular, $\alpha = 1$ (plane stress) was taken into account, together with the value of the constraint factor numerically calculated. Effective stress amplitudes, calculated considering the constraint factor calculated with FEM, are smaller than those calculated assuming plane stress conditions. This behavior is not in line with the experimental results, since it was observed that the opening loads recorded during small scale testing ($\alpha = 1$) were higher than those recorded during large scale tests: this means that the loading conditions considered in this study exceeds the limits of validity of the analytical model proposed by Newman.

It is also worth remarking that the effective stress ranges measured during the experiments were comparable to the total stress range, since crack opening levels were close to the applied minimum stress. From an engineering point of view, this means that a crack propagation model based on total stress and strain amplitudes can be implemented and provide

satisfactory results. These experimental observations, together with the da/dN–ΔJ_{eff} curve calculated in Section 4, were employed in the following section to provide a tool capable of assessing the fatigue lives of large scale specimens.

6. Fatigue life assessment for large scale specimens

Tests performed on small scale specimens highlighted the fact that experimental points lie on the reference da/dN–ΔJ_{eff} curve obtained testing a $C(T)$ specimen at $R = 0.7$, whereas the crack closure measurements performed on large scale specimens allowed an accurate estimation of the effective stress ranges experienced by the defect during propagation. This information, together with a correct formulation of ΔJ_{eff} range can be used to estimate the fatigue life of the large scale specimens.

This section is divided into two different parts. In the first, the analytical formulation of ΔJ is adapted to take into account large scale specimens geometry. A numerical model is then presented to validate the analytical expression. Finally, fatigue life of large scale specimens is assessed considering two different propagation models. A model based on the total ΔJ, interesting from an engineering viewpoint, is implemented and its estimates are compared to those proposed by the model which considers ΔJ_{eff}.

6.1. ΔJ formulation for large scale specimens

In this section, Eq. (1) was adapted to consider the geometry of large scale specimens. The concept of ΔJ was proposed by Dowling [8,41], who extended to fatigue the line integral originally introduced by Rice [7]. Cyclic J-Integral was implemented by replacing remote stress and strain with the remote stress and strain amplitudes cyclically applied to the cracked component. This feature, together with the fact that J can be computed only considering monotonic loadings, neglects the possibility to extract the value of ΔJ from numerical simulations. Accordingly, in this work the values of Y and $h(n_i)$ were calculated by considering a numerical model of a large scale specimen monotonically loaded.

The FEM model employed for α calculations was adopted: the geometric factor Y was calculated by considering material elastic behavior. For the given geometry, a value of 0.86 was obtained for the crack deepest point. This value differs less than 5% from the value calculated with the model proposed by Newman and Raju [42], meaning that, for large scale specimens, a good approximation of the geometric factor can be obtained from this set of equations, which considers a semi-elliptical crack in a plate subjected to axial and bending loads.

Material elastic–plastic behavior was introduced, to evaluate $h(n_i)$. Material inelastic behavior was modeled by adopting a power hardening law, as proposed in Eq. (6), in which Ramberg–Osgood equation is reported.

$$\epsilon = \epsilon_{el} + \epsilon_{pl} = \frac{\sigma}{E} + \left(\frac{\sigma}{k_i}\right)^{1/n_i} \tag{6}$$

During the simulation, the value of the applied force, F, was monotonically increased, to evaluate the trend of J. It was found that Eq. (1) best fits numerical results when the formulation of $h(n_i)$ proposed in Eq. (7) is adopted. This equation, originally proposed in [43], was calculated considering plane strain conditions.

$$h(n_i) = \frac{3}{4\sqrt{n_i}} \tag{7}$$

Numerically obtained coefficients were introduced in Eq. (1), as proposed in Eq. (8), in which plane strain conditions are assumed and Y_{NR} is the geometric factor calculated at crack deepest point according to Newman–Raju equations.

$$\Delta J = Y_{NR}^2 \pi a \left(\frac{\Delta\sigma^2(1-\nu^2)}{E} + \frac{3}{4\sqrt{n_i}}\Delta\sigma\Delta\epsilon_{pl}\right) \tag{8}$$

6.2. Fatigue life estimates

In this section, fatigue life of the four large scale specimens, tested under two different straining conditions, is assessed. The estimate is obtained by calculating the number of cycles necessary for the crack deepest point to propagate from the initial depth, a_0, measured after precracking, to the final defect size, a_f, measured after breaking the samples in liquid nitrogen.

An analytical procedure was implemented, in order to take into account material initial transient behavior. This was necessary because the values of $\Delta\sigma$ and $\Delta\epsilon_{pl}$, during initial fatigue cycles, are very different from those measured in the stabilized hysteresis loop. Moreover, this allowed the extraction of ΔJ directly from the stress/strain cycles, following original Dowling's proposal [8]. The steps considered in each iteration of the procedure are the following:

- calculation of the experimental stress and plastic strain amplitudes at the i-th load cycle, together with the strain power exponent n_i;
- evaluation of the applied ΔJ_i;
- computation of the i-th crack increment as:

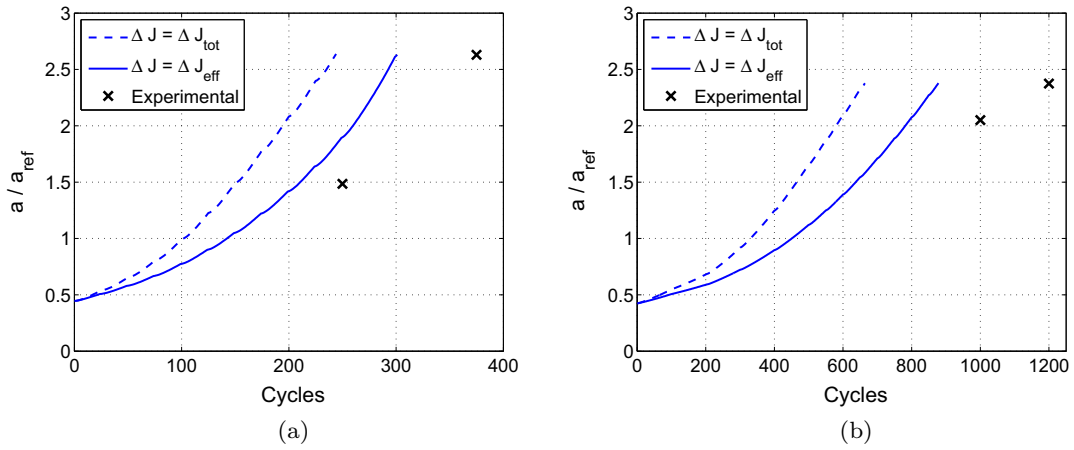

Fig. 15. Fatigue life assessment for the large scale specimens. Crosses represent experimental points, whereas the dashed and continuous lines are, respectively, the results of the simulations performed considering the models based on ΔJ_{tot} and ΔJ_{eff}. (a) $R = -1$ $\epsilon_a = 0.0035$ mm/mm; (b) $R = 0.5$ $\epsilon_a = 0.0025$ mm/mm.

$$da_i = C(\Delta J_i)^m \cdot \hat{dN}, \text{ with } \hat{dN} = 1 \tag{9}$$

where C and m are the constants that describe the closure-free propagation curve of the small scale specimens, shown in Fig. 10b.

– crack length update:

$$a_i = a_{i-1} + da_i \tag{10}$$

The changes of crack aspect ratio, a/c, where taken into account by updating, every iteration, the value of Y, which was calculated by considering the Newman–Raju equation. The value of the aspect ratio was changed linearly during the simulation, from the value registered after precracking to the one observed at the end of the test. This approximation was necessary, since it was not possible to experimentally evaluate the relationship between a and c.

Two different formulation of ΔJ were employed during calculations. Since the experimentally measured crack opening levels were very low, comparable to the minimum applied load, an initial model that considered ΔJ was adopted. According to this formulation, the total part of the stress and plastic strain ranges are considered in ΔJ calculations. Fatigue life assessment obtained considering ΔJ is represented in Fig. 15 by blue dashed lines. As expected, this formulation provides, for both the experiments, conservative results. This feature makes the model very interesting from an engineering point of view, since it provides conservative results with a relatively simple formulation.

As a further step in the analysis, the model based on ΔJ_{eff} was implemented. This model follows the formulation proposed by Vormwald [13], described in Section 2. In order to calculate the effective J-Integral range, $\Delta\sigma$ and $\Delta\epsilon_{pl}$ where replaced in Eq. (8) with the effective stress and plastic strain ranges, calculated as proposed in Eq. (4). Since it was not possible to evaluate crack closing levels (as displayed in Fig. 13), it was assumed that closing occurs at σ_{cl}, the stress level in which, during unloading, the strain at crack opening, ϵ_{op}, is reached, following what was experimentally observed on the small scale specimens.

Fatigue life assessment, obtained considering ΔJ_{eff} is represented in Fig. 15 by a continuous blue line. The adoption of the experimental effective stress and plastic strain ranges reduces the distance between the estimates and the experimentally observed fatigue life. The model provides conservative assessments for both the straining conditions investigated, underlining the capacity of ΔJ_{eff}-based models to describe crack propagation under LCF conditions.

7. Summary and conclusions

Fatigue crack growth under severe loading conditions was investigated for a linepipe steel. A preliminary experimental campaign was performed on specimens containing 400 μm deep semi-circular defects, in order to observe fatigue crack growth. Two different loading conditions were investigated. Specimens were initially tested with a fixed strain ratio, R, equal to −1, with an applied strain amplitude, ϵ_a, equal to 0.0035 mm/mm, to check the ΔJ_{eff}-based model employed to describe crack growth. At this point, the strain ratio was changed to 0.5 and ϵ_a to 0.0025 mm/mm, in order to check crack propagation with selected straining conditions. Experimental results were analyzed in terms of crack growth rates, considering the analytical model proposed by Newman, and were compared to those obtained testing a C(T) specimen at an high stress ratio ($R = 0.7$). It was observed that experimental crack growth rates were higher than those measured during long crack testing. Therefore, a new series of experiments was performed on the same specimen geometry, in order to check crack-closure. An

innovative experimental technique, based on digital image correlation, was employed to measure crack opening levels. The technique consisted in applying a virtual strain gauge under the defect: crack opening and closing levels were evaluated as the points in which the stress/strain cycle measured by the virtual gauge differed from the remote one, measured by the extensometer which controlled the strain amplitude applied to the specimen.

DIC-based measurements showed that the analytical opening levels, calculated with the model proposed by Newman, were higher than those experimentally observed: this means that the value of ΔJ_{eff} calculated with the model underestimated the real crack propagation driving force. At this point, the propagation model was modified to take into account measured crack closure levels: experimental data points shifted on the da/dN–ΔJ_{eff} obtained from C(T) testing.

A different specimen geometry was then taken into account. Specimens with a 43 mm $\times$ 10 mm net section were tested with the same loading conditions applied on the small specimens, in order to check crack propagation in different consortaint conditions. In this phase, 0.7 mm deep defects were considered. Crack opening levels were measured during propagation, with the same technique employed for the small specimens. Smaller crack opening levels were observed: this was related to the difference in the constraint factor between the two considered geometries.

Finally, the crack propagation model was employed to assess fatigue life of large scale specimens: ΔJ equation was adapted in order to take into account the geometry of large scale specimens. A numerical model was employed to confirm the proposed formulation, showing that, for the large scale geometry, the plastic part of the J-Integral can be modelled considering a plane strain condition. It was found that a fatigue life assessment based on ΔJ provides very conservative results, with a factor of 2 respect to experiments, whereas an approach based on ΔJ_{eff} provides 25% conservative predictions.

Acknowledgements

Dr. Mario Rossi, director of Tenaris Dalmine Research and Development Center, and Dr. Philippe Darcis, Linepipe Product Manager, are kindly acknowledged for the permission to publish this paper.

References

[1] Izquierdo A, Quintanilla H, Richard G, Garcia E, Armengol M, Novelli P, et al. Development of line pipe for high pressure/high temperature and sour service applications. In: Proc. of offshore and arctic engineering, OMAE2009-79153; 2009.
[2] Di Vito L, Mannucci G, Mortali G, Armengol M, Novelli P, Izquierdo A, et al. Ultra heavy wall linepipe x65: material performances for severe applications. In: ASME 2009 28th international conference on ocean, offshore and arctic engineering. American Society of Mechanical Engineers; 2009. p. 145–58.
[3] Di Vito L, Ferino J, Mannucci G, Lucci A, Vitali L, Marchesani F, et al. Ultra heavy wall linepipe x65: ratcheting in severe cyclic straining. In: ASME 2010 29th international conference on ocean, offshore and arctic engineering. American Society of Mechanical Engineers; 2010. p. 899–910.
[4] Cristea M, Beretta S, Altamura A. Fatigue limit assessment on seamless tubes in presence of inhomogeneities: small crack model vs. full scale testing experiments. Int J Fatigue 2012;41:150–7.
[5] Miller K, Murakami Y. What is fatigue damage? a view point from the observation of low cycle fatigue process. Int J Fatigue 2005;27(8):991–1005.
[6] Miller K. Materials science perspective of metal fatigue resistance. Mater Sci Technol 1993;9(6):453–62.
[7] Rice JR. A path independent integral and the approximate analysis of strain concentration by notches and cracks. J Appl Mech 1968;35(2):379–86.
[8] Dowling N. Cyclic stress–strain and plastic deformation aspects of fatigue crack growth. ASTM; 1977.
[9] Paris P, Erdogan F. A critical analysis of crack propagation laws. Basic Engng Trans ASME Ser D 1963;85:528–34.
[10] Zezulka P, Polak J. Short crack growth and fatigue life in austenitic-ferritic duplex stainless steel. Fatigue Fract Engng Mater Struct 2005;28 (10):923–35.
[11] Härkegård G, Denk J, Stärk K. Growth of naturally initiated fatigue cracks in ferritic gas turbine rotor steels. Int J Fatigue 2005;27(6):715–26.
[12] Skallerud B, Zhang Z. A 3D numerical study of ductile tearing and fatigue crack growth under nominal cyclic plasticity. Int J Solids Struct 1997;34 (24):3141–61.
[13] Vormwald M, Seeger T. The consequences of short crack closure on fatigue crack growth under variable amplitude loading. Fatigue Fract Engng Mater Struct 1991;14(2/3):205–25.
[14] Radaj D, Vormwald M. Elastic–plastic fatigue crack growth. In: Advanced methods of fatigue assessment. Springer; 2013. p. 391–481.
[15] Vormwald M. Effect of cyclic plastic strain on fatigue crack growth. Int J Fatigue 2015.
[16] McClung R, Sehitoglu H. Closure behavior of small cracks under high strain fatigue histories. In: Newman J, Elber W, editors. Mechanics of fatigue crack closure. ASTM; 1988. p. 279–99 [chapter 2].
[17] McClung R, Sehitoglu H. Characterization of fatigue crack growth in intermediate and large scale yielding. J Engng Mater Technol 1991;113:15–22.
[18] Pippan R, Grosinger W. Fatigue crack closure: from lcf to small scale yielding. Int J Fatigue 2013;46:41–8.
[19] Rabbolini S, Beretta S, Foletti S, Riva A. Short crack propagation in lcf regime at room and high temperature in q & t rotor steels. Int J Fatigue 2015;75:10–8.
[20] Newman J. A crack-closure model for predicting fatigue crack growth under aircraft spectrum loading. In: Chang J, Hudson C, editors. Methods and models for predicting fatigue crack growth under random loading. ASTM; 1981. p. 53–84.
[21] Peters W, Ranson W. Digital imaging techniques in experimental stress analysis. Opt Engng 1982;21(3):213427.
[22] Sutton M, Wolters W, Peters W, Ranson W, McNeill S. Determination of displacements using an improved digital correlation method. Image Vision Comput 1983;1(3):133–9.
[23] Peters W, Ranson W, Sutton M, Chu T, Anderson J. Application of digital correlation methods to rigid body mechanics. Opt Engng 1983;22(6):226738.
[24] Chu T, Ranson W, Sutton M. Applications of digital-image-correlation techniques to experimental mechanics. Exp Mech 1985;25(3):232–44.
[25] Sutton MA, Zhao W, McNeill SR, Helm JD, Piascik RS, Riddell WT. Local crack closure measurements: development of a measurement system using computer vision and a far-field microscope. ASTM Special Technical Publication 1343; 1999. p. 145–56.
[26] Riddell W, Piascik R, Sutton M, Zhao W, McNeill S, Helm J. Determining fatigue crack opening loads from near-crack tip displacement measurements. ASTM Special Technical Publication 1343; 1999. p. 157–74.
[27] Carroll J, Efstathiou C, Lambros J, Sehitoglu H, Hauber B, Spottswood S, et al. Investigation of fatigue crack closure using multiscale image correlation experiments. Engng Fract Mech 2009;76(15):2384–98.
[28] Pataky GJ, Sangid MD, Sehitoglu H, Hamilton RF, Maier HJ, Sofronis P. Full field measurements of anisotropic stress intensity factor ranges in fatigue. Engng Fract Mech 2012;94:13–28.

[29] Rabbolini S, Pataky GJ, Sehitoglu H, Beretta S. Fatigue crack growth in haynes 230 single crystals: an analysis with digital image correlation. Fatigue Fract Engng Mater Struct 2015;38:583–96.
[30] Tomkins B. Fatigue crack propagation – an analysis. Philos Mag 1968;18(155):1041.
[31] R6. Assessment of the integrity of structures containing defects. British Energy Generation Ltd.; 2000.
[32] Beretta S, Foletti S, Rabbolini S, Bordo LE, Sanguineti A, Traversone L. Models for small crack growth in lcf at room temperature and high temperature. In: ASME Turbo Expo 2012: turbine technical conference and exposition. American Society of Mechanical Engineers; 2012. p. 323–30.
[33] Dowling N, Begley J. Fatigue crack growth during gross plasticity and the j-integral. In: Mechanics of crack growth. ASTM; 1976. p. 82–103.
[34] Paravicini Bagliani E, Anelli E, Paggi A, Di Cuonzo S. Development of heavy wall seamless pipes with improved toughness and hardness control. In: 6th Int. pipeline technology conference; 2013.
[35] Farè S, Ortolani M, Paravicini Bagliani E, Crippa S, Novelli P, Darcis P. Mechanical properties and weldability of ultra-heavy wall seamless pipes for sour and arctic-alike environment. In: ISOPE-2015 25th international offshore and polar engineering conference; 2015.
[36] Newman Jr J, Schneider J, Daniel A, McKnight D. Compression pre-cracking to generate near threshold fatigue-crack-growth rates in two aluminum alloys. Int J Fatigue 2005;27(10):1432–40.
[37] Larsen JM, Allison JE. Small-crack test methods, vol. 1149. Astm International; 1992.
[38] Pataky GJ, Sehitoglu H, Maier HJ. High temperature fatigue crack growth of haynes 230. Mater Character 2013;75:69–78.
[39] Savaidis G, Dankert M, Seeger T. An analytical procedure for predicting opening loads of cracks at notches. Fatigue Fract Engng Mater Struct 1995;18 (4):425–42.
[40] Newman Jr J, Bigelow C, Shivakumar K. Three-dimensional elastic-plastic finite-element analyses of constraint variations in cracked bodies. Engng Fract Mech 1993;46(1):1–13.
[41] Dowling N. J-integral estimates for cracks in infinite bodies. Engng Fract Mech 1987;26(3):333–48.
[42] Newman Jr J, Raju I. An empirical stress-intensity factor equation for the surface crack. Engng Fract Mech 1981;15(1):185–92.
[43] He M, Hutchinson J. The penny-shaped crack and the plane strain crack in an infinite body of power-law material. J Appl Mech 1981;48(4):830–40.